



# Broadband Antipodal Vivaldi Antenna With Simultaneous Flat Gain and Filtering Characteristic

Xiaochun Shao<sup>1</sup> · Lianwen Deng<sup>1</sup> · Chengxi Zhou<sup>1</sup> · Tianyi Yan<sup>1</sup> · Chao Tang<sup>1</sup> · Xiaohui Gao<sup>1</sup> · Lei-Lei Qiu<sup>1</sup> 

Received: 24 July 2022 / Accepted: 29 December 2022 / Published online: 4 January 2023  
© King Fahd University of Petroleum & Minerals 2023

## Abstract

A broadband antenna with simultaneous flat gain and filtering characteristic is proposed in this paper. To achieve a flat gain response, rectangle slots and a bandpass filter are loaded on the antipodal Vivaldi antenna. The loaded rectangle slots adjust the phase of the surface currents to widen the operating bandwidth, as well as reduce the far-field radiation cancellation of the reverse currents in the end-fire direction, thus improving the gain. In addition, a bandpass filter is added to the antenna to further equalize the currents amplitude and suppress out-of-band signals. The measured results show that the proposed antenna achieves an impedance bandwidth of 101.9% (3.99–12.28 GHz) and an out-of-band suppression level of 15.5 dBi in the upper stopband. What is more, an extremely low gain fluctuation of  $\pm 0.464$  dBi is realized in the 4–12 GHz. Compared with conventional broadband antennas, the antenna features simple structure and better performance, which achieves broadband with simultaneous flat gain response and filtering characteristic. The proposed antenna may be applied in high-precision radar sensing system.

**Keywords** Broadband antenna · Phase · Amplitude · Filtering · Flat gain

## 1 Introduction

In recent years, broadband antenna has attracted extensive attention as their excellent ability to carry a wider working bandwidth. The design emphasis of broadband antenna is to balance the stable radiation pattern, good impedance matching, and few gain fluctuation in the whole bandwidth. However, for antennas, flat gain and broadband are mutual restraint with each other, so how to obtain a broadband antenna with flat gain is one of the main challenges in the research of broadband antennas, especially in high-precision radar sensing system.

For purpose of broadening the impedance bandwidth of antennas, many approaches have been proposed. Firstly, increasing the thickness or decreasing the relative dielectric constant of the substrate is a common method to expand bandwidth [1, 2]. In [3], a four-layer dielectric substrate was used to obtain a center frequency of 15 GHz and 30% relative

bandwidth, but its size was relatively large with a gain fluctuation of more than  $\pm 1.75$  dBi. Secondly, feeding structure is the key factor of impedance matching [4–8]. A pair of differential fed were developed to excite the antenna, achieving a center frequency of 7.3 GHz and relative bandwidth of 132%, but its gain fluctuation was  $\pm 3.55$  dBi [9]. Alternatively, impedance matching can be enhanced by modifying the antenna radiation unit shape [10–18]. An improved antipodal Vivaldi antenna with a center frequency of 9.15 GHz and a bandwidth of 171.2% was obtained by using two pairs of tapered slots and circularly shaped loads, with a gain fluctuation of  $\pm 2.9$  dBi [19]. Also, the addition of parasitic patch can introduce new resonant frequency to the antenna, thus enhancing the impedance bandwidth [20–23]. However, the broadband antennas mentioned above still have relatively large gain fluctuation.

To reduce the fluctuation in antenna gain, the researchers came up with several methods. The first method is changing the shape of the antenna radiation unit to obtain flat gain [24, 25]. In [26], the non-uniformly segmented dipole antenna obtained an in-band gain fluctuation of  $\pm 1.1$  dBi by weakening the reverse currents in the long dipole arms, with a relative bandwidth of 66.2%. In addition, the traditional antipodal Vivaldi antenna achieved a gain fluctuation of  $\pm 1.1$  dBi and

✉ Lei-Lei Qiu  
qiuleilei@csu.edu.cn

<sup>1</sup> School of Physics and Electronics, Central South University, Changsha 410083, China



a working bandwidth of 114.3% by loading a pair of open stubs, comb-shaped slot array, and semi-elliptical patches [27]. This method is convenient to realize wide band, but the gain fluctuation is still large. For the second approach, some scholars presented to stabilize antenna gain response by loading a phase adjusting element in the main radiation direction [28, 29]. In [30], a flexible three-dimensional (3-D) phase adjusting unit lens loaded in front of a conventional Vivaldi antenna is developed, with a gain fluctuation about  $\pm 1$  dBi in 100% bandwidth when the phase adjusting unit is bended outward. However, it causes a more complex structure and larger size for the antenna. The last method uses the filtering characteristic to equalize the in-band gain amplitude to achieve a smaller gain fluctuation [31–34]. The designed filtering antenna in [35] achieved an in-band gain fluctuation of  $\pm 0.5$  dBi, but obtained the fractional bandwidth of only 22.6%. Till now, it is still a challenge to explore a broadband antenna with simultaneous flat gain, broadband, and filtering characteristics by using a simple structure.

To address the above-mentioned issue, an improved antipodal Vivaldi antenna is proposed based on the method of phase and amplitude equalization. For this purpose, rectangle slots are loaded on the antenna to adjust the currents phase, broadening operating band to cover CX-band and weakening the gain cancellation caused by the reverse currents, thus improving the antenna gain. Moreover, considering that filtering structure features equalizing currents amplitude and suppressing out-of-band signals, adding a bandpass filtering structure to the antenna can further flatten the gain response. The measured results show that the proposed antenna not only realizes a gain fluctuation about  $\pm 0.464$  dBi in CX-band but also features an out-of-band suppression level of 15.5 dBi in the upper stopband.

The remainder of this paper is organized as follows. The working principle and investigation of phase regulation, amplitude equalizing of the proposed antenna are illustrated in Sect. 2. To validate the design approach, a prototype antenna is fabricated and measured as presented in Sect. 3, and conclusions are given in Sect. 4.

## 2 Antenna Structure and Analysis

The reference antenna proposed in this paper consists of a broadband balun and a main elliptical radiator, as shown in Fig. 1a. The dielectric substrate of the antenna is Rogers RO3003, which has a permittivity of 3, a dielectric loss tangent of 0.0013, and a thickness of 1.524 mm. A microstrip line with  $50 \Omega$  impedance is transformed into parallel strip line with a gradual ground to form a broadband balun, which is then connected with the radiation arms to achieve the broadband reference antenna. A miniaturized filtering structure, as displayed in Fig. 1b, is cascaded to the

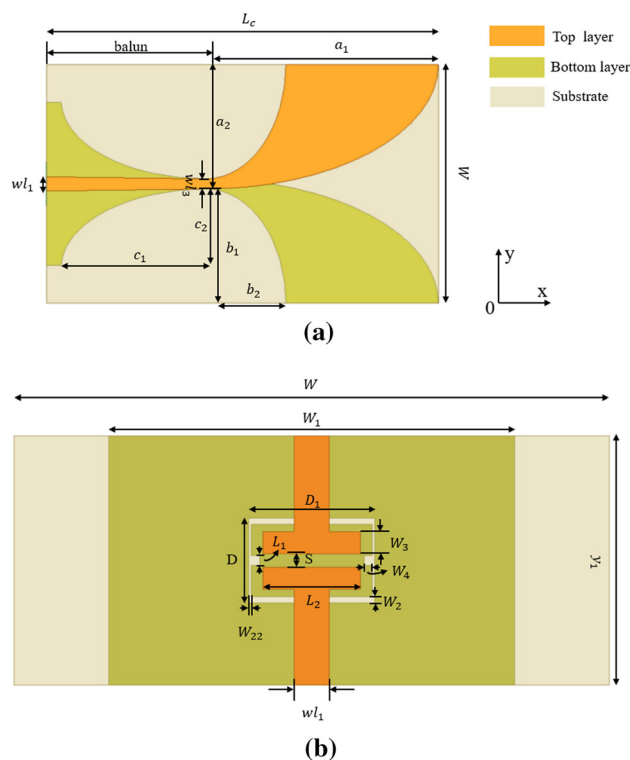
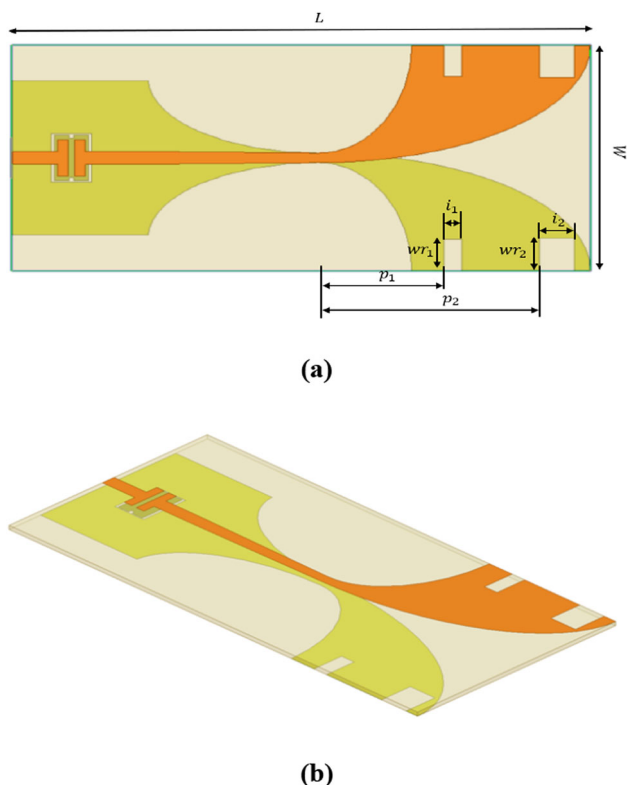


Fig. 1 **a** Reference antenna geometry, **b** filtering structure

above-mentioned antenna for the purpose of equalizing gain amplitude and improving out-of-band selectivity. As can be seen in Fig. 2, the finally constructed antenna is also etched with several rectangular slots to adjust the phase of the surface currents on the arms. As a result, the proposed antenna has flat gain response and filtering characteristic, simultaneously.

### 2.1 Broadband Balun

For the proposed Vivaldi antenna, the balun plays an important role in improving its operating bandwidth. The geometry of the balun is depicted in Fig. 1a, which is composed of a rectangular ground with a pair of ellipses slots printed on the bottom surface of the substrate, and a microstrip line loaded on the top surface. To have high efficiency transmission from microstrip line to parallel strip line, as well as continue into radiation arms, the width of the microstrip line and the size of the ground is very critical. In the simulation of the balun  $S$ -parameters, the loss of the dielectric substrate has a significant impact on the total insertion loss of the balun relative to the conductor loss, so the loss of the dielectric substrate has been considered in the simulation with loss tangent of 0.0013. Parameters analysis is conducted here to enable the transmission bandwidth of the balun cover the designed CX-band. Its final  $S$ -parameters are provided in



**Fig. 2** Proposed antenna geometry ( $a_1 = 64, a_2 = 34.4, b_1 = 31.6, b_2 = 22, c_1 = 40, c_2 = 22, w_{l1} = 3.9, w_{l3} = 2.8, L = 136, L_c = 108, y_1 = 28, W = 66, W_1 = 45, D = 9.5, D_1 = 14, S = 1.5, L_1 = 0.9, L_2 = 10.8, W_2 = 0.7, W_{22} = 0.2, W_3 = 2.5, W_4 = 1.1, i_1 = 4.2, i_2 = 8.2, w_{r1} = 9.2, w_{r2} = 9.6, p_1 = 29.5, p_2 = 52$ , unit: mm): **a** Top view, **b** 3D view

**Fig. 3.** Good impedance matching and relatively stable transmission coefficient ( $|S_{21}|$ ) are achieved within 4–12 GHz. Then, the broadband balun is connected with the antenna radiating arms to achieve the broadband reference antenna.

**2.2 Phase Regulation**

The radiation principle of antipodal Vivaldi antenna is that the energy is coupled to the radiation arms through the microstrip line and then flows to the end of opening direction on the inner edges of the radiation arms. To illustrate the mechanism more clearly, the currents on the radiation arms are considered to be decomposed into the  $x$ -axis (the end-fire direction) and the  $y$ -axis components (the vertical direction of the end-fire direction). Since the  $x$ -axis components of the currents in the two radiation arms are always  $180^\circ$  difference, their far-field radiation in the end-fire direction nearly cancels each other out. Therefore, what actually effects the antenna gain is the superposition of the far-field radiation of the  $y$ -axis components of the currents in the  $x$ -axis direction. Meanwhile, the ground plane reflects the radiation generated by the  $y$ -axis components to enhance the far-field radiation in the end-fire

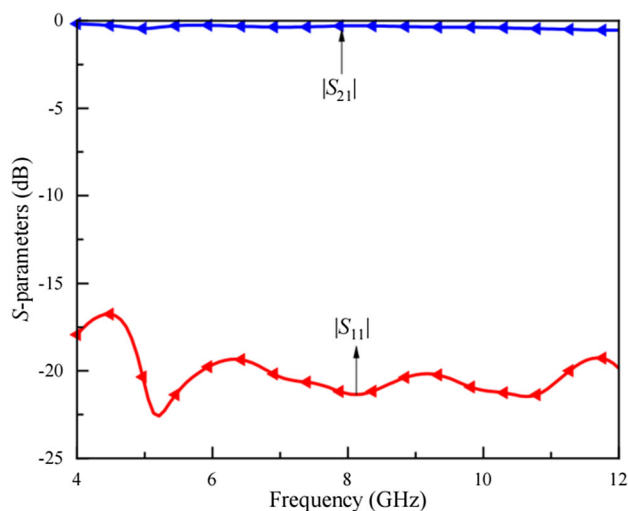


**Fig. 3** Simulated  $S$ -parameters of balun

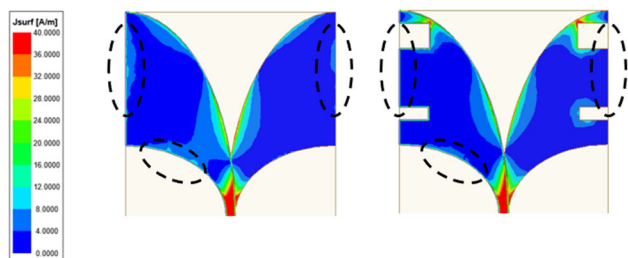


**Fig. 4** Current amplitude distributions on the antenna at 4 GHz **a** without slots, **b** with slots

direction. In fact, the currents in the radiation arms are relatively scattered. Some of the currents flow to the outside of the radiation arms, which increases the  $x$ -axis components and weakens that in the  $y$ -axis direction, resulting in an increase of the side lobes and the instability of the radiation pattern. Further, it causes the antenna dramatic gain fluctuation over the operating bandwidth. To stabilize the in-band gain performance, two pairs of rectangle slots along the  $y$ -axis are loaded on the radiation arms to suppress the  $x$ -axis components of the currents, while increase the  $y$ -axis components.

To explain the function of slots more clearly, the surface currents amplitude distributions of the antenna at 4 GHz without slots and with slots are depicted in Fig. 4. The antipodal Vivaldi antenna concentrates the current at the inner edges of the radiating arms by the coupling between the radiating arms and produces radiation pointing in the end-fire direction. However, the distance of the area near the end opening of the radiating arms results in a weaker coupling between the radiating arms, so some current hardly flows along the inner edges of the radiating arms and the current distribution is more dispersed. As shown in Fig. 4a, the circled part has some current outside the radiating arms, resulting in a weaker

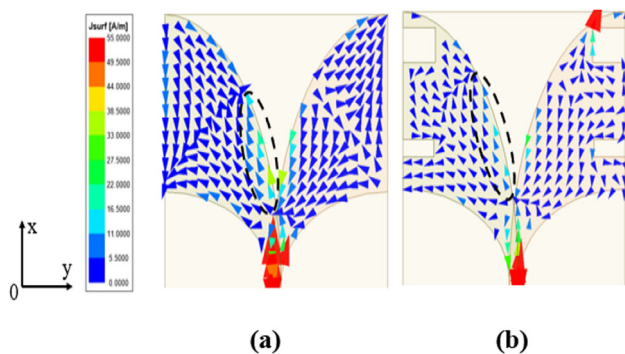
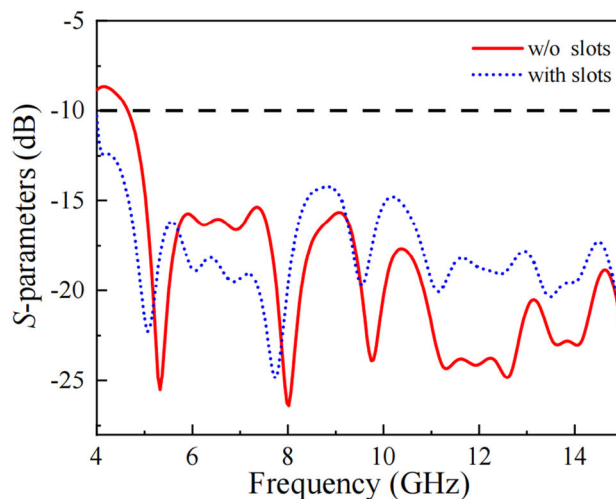


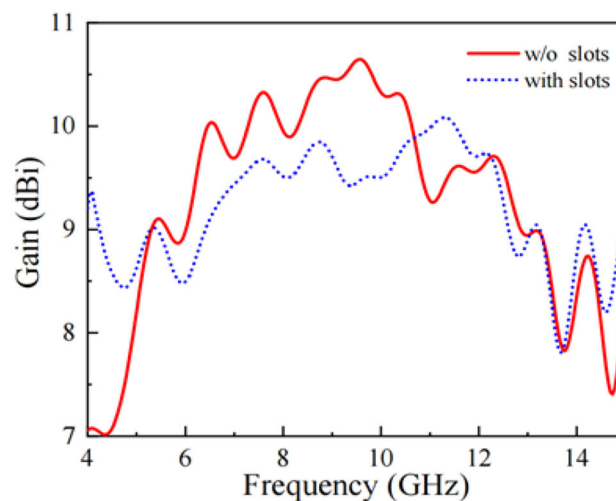
**Fig. 5** Current vector distributions on the antenna at 4 GHz: **a** without slots, **b** with slots

current density on the inner edges of radiating arms. However, after loading rectangular slots on the radiating arms, the current as marked in the circle is effectively suppressed, promoting the current on the radiating arms to concentrate on the inner edges, as depicted in Fig. 4b. Especially at the end opening position of radiating arms, the current density is significantly stronger than that of antenna without slots. Similarly, in Fig. 5a, part of the current vector on the radiating arms flows along the  $x$ -axis direction to the outside of the radiation arms, weakening the intensity of the current vector on the inner edges of the radiation arms. When loading rectangular slots paralleling to the  $y$ -axis on the antenna radiating arms, the rectangular slots obstruct the current flowing to the outside the antenna radiating arms, which changes the traveling path of the current vector, so that the current is forced to gather near the inner edges of the radiating arms, as depicted in Fig. 5b. Particularly in the vicinity of the rectangular slots near the end of the radiating arms, the current vector would resonate strongly and be significantly enhanced, causing the current being aggregated around the position between the rectangular slots and the inner edges of the radiating arms, thus achieving an effective extension of the low frequency impedance bandwidth and improving the directional radiation performance of the antenna. In addition, the currents along the  $x$ -axis are obviously restrained, but the currents along the  $y$ -axis are enhanced significantly.

When the currents distribution is chaos, the unwanted radiation is excited from the surface currents of the antenna. This radiation leads to gain reduction, side lobes increasing, and pattern distortion, so the antenna gain is closely related to the currents phase. When the antipodal Vivaldi antenna works at different frequencies, the radiation arms have reverse currents with different distances related to the free space half-wavelength of the working frequencies, and the corresponding  $y$ -axis components of the currents affecting the antenna gain also feature same periodic distributions. According to the theory of antenna array, the far-field radiation of the current elements in reverse phase separated by



**(a)**



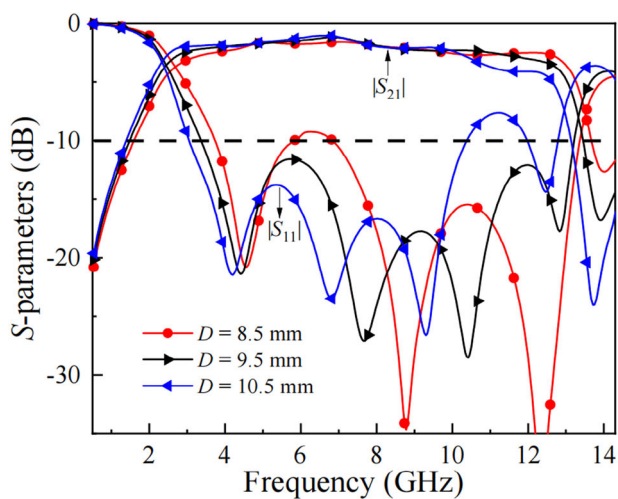
**(b)**

**Fig. 6** Simulated results of reference antenna without and with slots: **a**  $|S_{11}|$ , **b** Gain

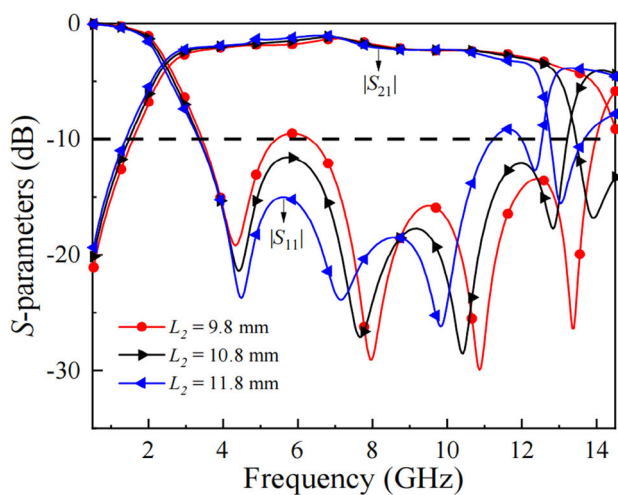
half-wavelength will produce a superposition impact in the end-fire direction of the antenna. In order to improve the gain, the distances between the reverse current elements need to close to half-wavelength. Otherwise, they will cancel each other out, reducing the gain. Consequently, etching slots on the radiation arms with a reasonable distance, the currents phase can be adjusted, which further redistribute the  $y$ -axis components of the currents.

To better understand the role of rectangular slots on the current phase, vector distributions of antenna currents without and with slots are carefully studied, as shown in Fig. 5. The ellipse circumference is

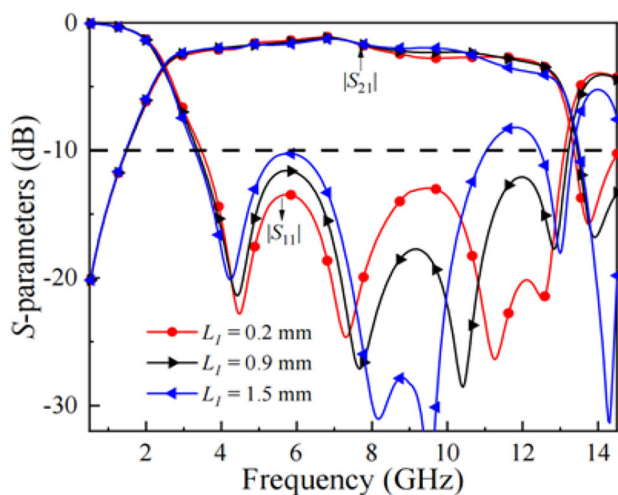
$$L = 2 * \pi * b + 4 * (a - b) \quad (1)$$



(a)

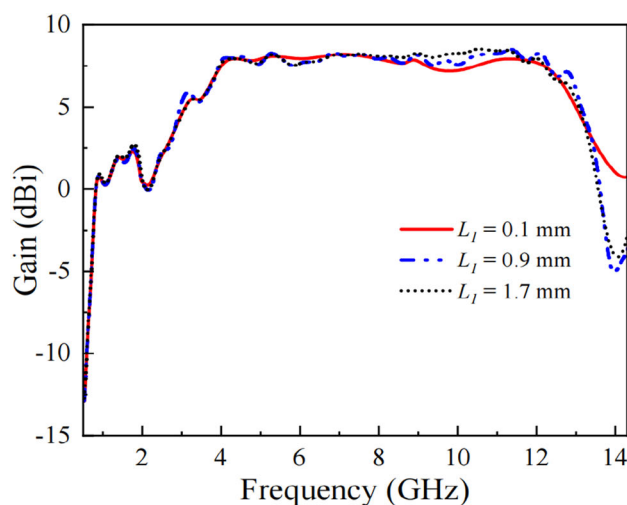


(b)

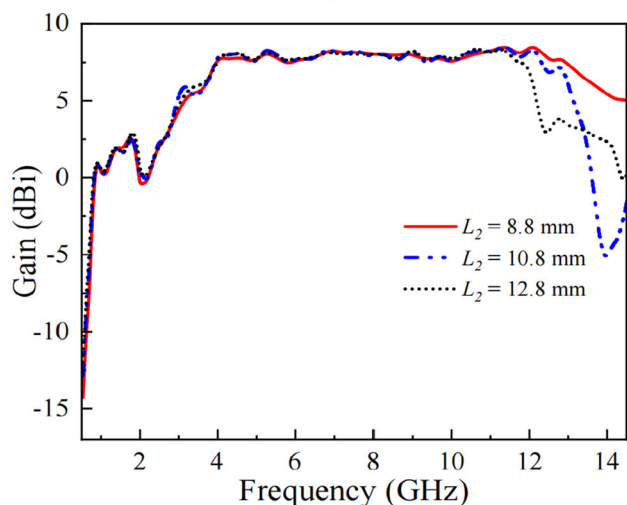


(c)

Fig. 7 Simulated S-parameters of filtering structure: a D, b L2, c L1



(a)



(b)

Fig. 8 Simulated gain of proposed antenna: a L1, b L2

$$W \geq \frac{c}{2 * f_L} \tag{2}$$

$$f_{L1} = \frac{c}{\lambda_1 * \sqrt{\epsilon_r}} \tag{3}$$

$$f_{L2} = \frac{c}{\lambda_2 * \sqrt{\epsilon_r}} \tag{4}$$

where  $a$  is the long axis of the ellipse about  $a = a_1 = 64$  mm and  $b$  represents the short axis of the ellipse, that is,  $b = a_2 = 34.4$  mm. Due to the radiation arms of the reference antenna accounting for 1/4 of the entire ellipse, the inner circumference of the radiation arms can be obtained according to (1), i.e.,  $L/4 = 83.61$  mm. From the currents vector distributions, it is approximately calculated that the distance between the reverse currents of the antenna without slots is 30.96 mm, as



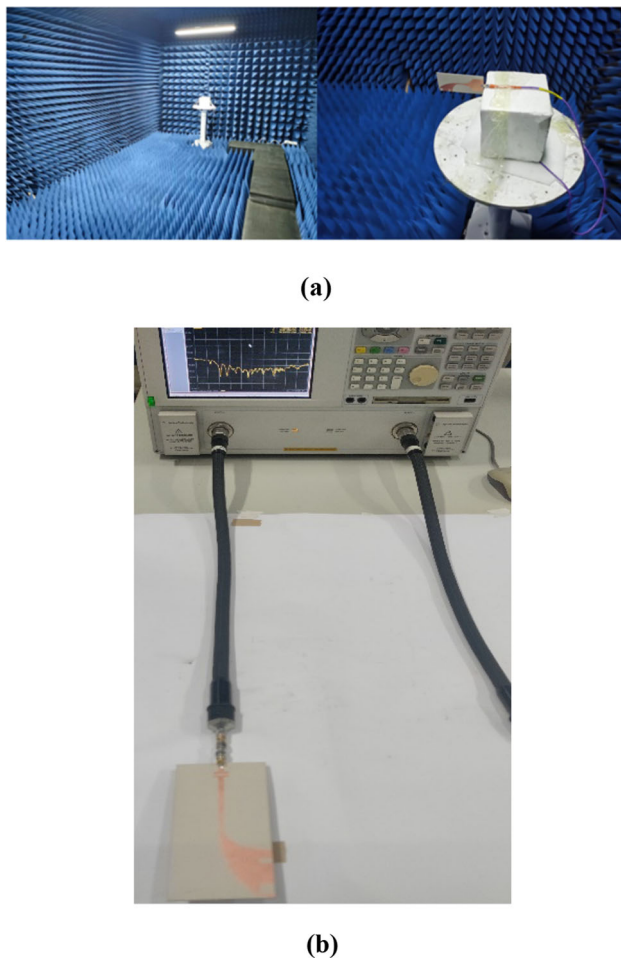


**Fig. 9** a The experimental platform and the fabricated sample, b  $S_{11}$  of proposed antenna measured by vector network analyzer

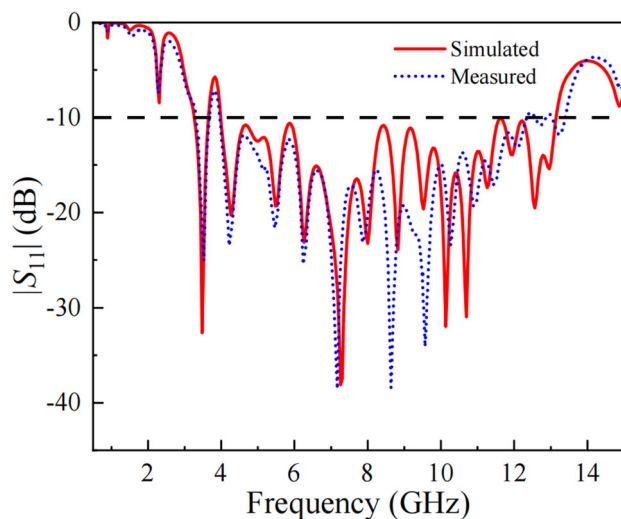


**Fig. 10** Measured and simulated reflection coefficient of the proposed antenna

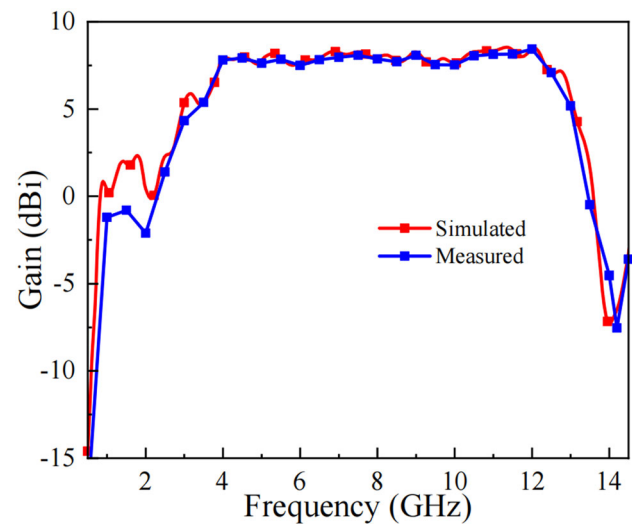


**Fig. 11** Measured and simulated gain of the proposed antenna

circled in Fig. 5a at 4 GHz, which is less than  $37.5$  mm of the free space half-wavelength ( $\lambda_0/2$ ) at 4 GHz. Therefore, more reverse currents cancel each other out in the far-field of the antenna, resulting in a decrease in gain and a gain of  $7.05$  dBi, as can be seen from Fig. 6b. After loading slots, the distance between the reverse currents on the antenna is  $37.7$  mm, which is more close to half-wavelength  $37.5$  mm, as circled in Fig. 5b. Therefore, the far-field radiation of surface reverse currents in the end-fire direction will mainly realize a superposition effect, and its gain is about  $9.2$  dBi at 4 GHz from Fig. 6b. According to the theory in [36], the end opening width of the conventional antipodal Vivaldi antenna must be more than  $\lambda/2$  corresponding to the low cutoff frequency in free space, which is expressed as Eq. 2, where  $c$  is the electromagnetic wave velocity in free space, and  $f_L$  takes 4 GHz, so  $W$  can be obtained as greater than or equal to  $37.5$  mm. After parameter scanning, the final size of end opening width of the antenna  $W$  is  $66$  mm, which satisfies Eq. 2, and thus the impedance bandwidth of 4–12 GHz can be achieved in theory. Another respect, etching slots on the radiation arms can be regarded as introducing half-wavelength dipoles with lengths of  $9.6$  mm and  $9.2$  mm, which approximately correspond to the  $1/4$  of the free space working wavelength of  $4.13$  GHz and  $5$  GHz, respectively, which meets Eq. 3 and Eq. 4, where  $\epsilon_r$  is the relative permittivity of the dielectric substrate Rogers RO3003 of 3. As shown in Fig. 6b, the low-frequency gain achieves an improvement after slots being loaded. Finally, the antenna gain response in the whole operating band is more smooth and the gain fluctuation is about  $\pm 0.82$  dBi.

Based on the above analysis, loading slots on the antenna radiation arms can adjust the surface currents phase and enhance radiation, thus improving the gain performance of the antenna for lower gain fluctuation.

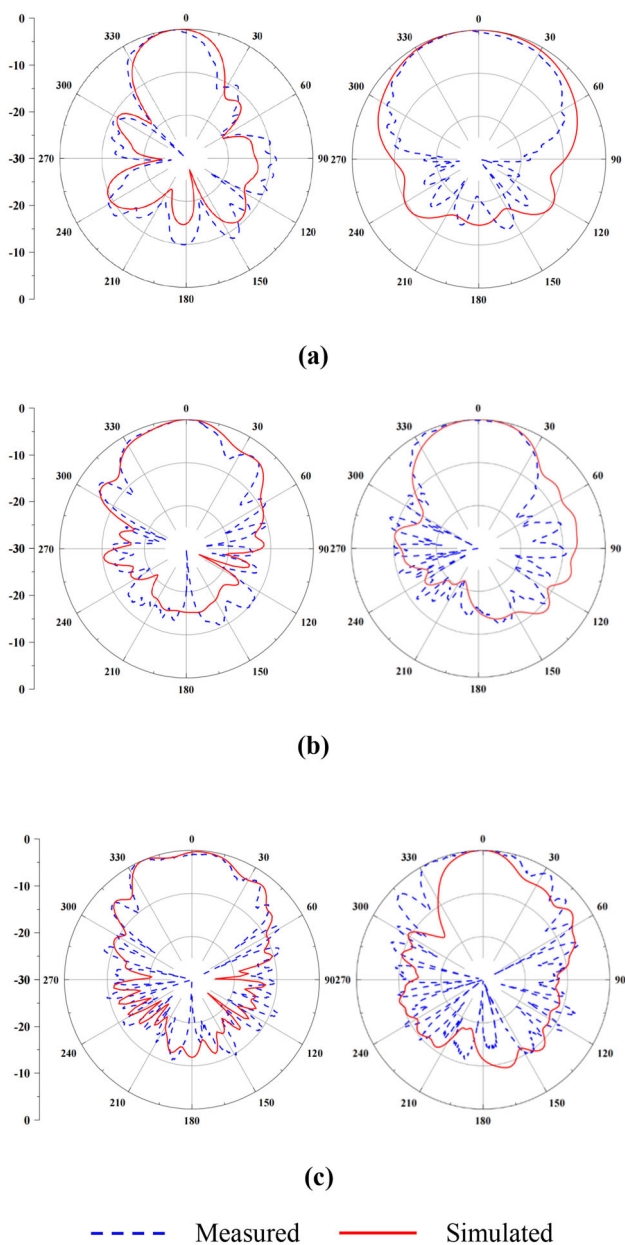


**Fig. 12** Measured and simulated H-plane and E-plane radiation patterns of the proposed antenna, **a** 4 GHz, **b** 8 GHz, **c** 12 GHz (Unit: dB)

### 2.3 Amplitude Equalizing

According to Sect. 2.2, the antenna gain fluctuation is still large and the out-of-band high frequency gain is still high. From the perspective of the currents amplitude, cascading a filtering structure to the antenna can further equalize the gain response, as well as introduce a transmission null in the upper stopband to suppress the high frequency out-of-band signals of the antenna.

$$f_0 = \frac{c}{4 * D} \tag{5}$$

The main dimensional parameter  $D$  of the filtering structure is set as quarter wavelength corresponding to the passband center frequency  $f_0$ . From Eq. 5, when  $D$  takes 9.5 mm,  $f_0$  is approximately computed as 7.89 GHz, which is similar to the simulated value of 7.65 GHz. After appropriate tuning, three resonant frequencies as 4.34, 7.72, and 10.36 GHz, corresponding to three modes of the SLR respectively, are obtained covering a transmission bandwidth of 4–12 GHz. As depicted in Fig. 7a, when the value of  $D$  increases from 8.5 to 10.5 mm, the transmission bandwidth gradually decreases, and the resonant frequencies shift downward. Attributed to the electromagnetic coupling between the parallel microstrip line and the SLR, where the currents flow in opposite directions and thus cancel each other, a transmission null is generated in the upper stopband. The transmission null mainly depends on the parallel line length  $L_2$ . When the  $L_2$  length increases from 9.8 to 11.8 mm as shown in Fig. 7b, the transmission null shifts toward lower frequency. With the increasing of shorted slot-line stubs length  $L_1$ , the far-field cancellation is enhanced at the transmission null, while with lower in-band ripple, as shown in Fig. 7c. Therefore, the pass-band bandwidth and the out-of-band suppression level can be controlled by tuning the filter parameters.

### 2.4 Proposed Antenna

Combined the methods of phase regulation and amplitude equalizing, the proposed antenna is readily developed. Figure 8 shows the gain response of the antenna against different  $L_1$  and  $L_2$ . It can be seen from Fig. 8a that the shorted slot-line stubs length has a more significant influence on the in-band gain fluctuation and the null. The in-band gain fluctuation decreases but the out-of-band suppression level at null frequency will first increase and then decrease, as the  $L_1$  gets longer. Therefore, a compromise between the in-band ripple and the suppression level is needed. It is found in Fig. 8b that the length  $L_2$  has an obvious effect on the null but hardly effects the gain response. The null shifts downward and the out-of-band suppression level in the upper stopband deteriorates with an increase for value of  $L_2$ . Therefore, after an appropriate design of the parameters, a broadband antenna with simultaneous flat gain and filtering characteristic is finally achieved.

## 3 Results and Discussion

To verify the design method, the proposed antenna is designed and fabricated. The electromagnetic simulation software HFSS is used. The fabricated sample is shown in Fig. 9, which is measured by a vector network analyzer (Agilent Technologies N5230A) in a microwave anechoic chamber.

**Table 1** Comparison other broadband and filtering antennas

Ref	Thickness ( $\lambda_0$ ) $\lambda_0$ at center freq. (mm)	Relative bandwidth (%)	Gain fluctuation (dBi)	Average gain (dBi)	Filtering	No. of radiation nulls
[15]	0.0284	175.58	$\pm 2$	8	No	0
[19]	0.0244	171.2	$\pm 2.9$	6.4	No	0
[21]	0.3837	72.7	$\pm 1.45$	7.32	No	0
[26]	0.1562	66.2	$\pm 1.1$	3.1	No	0
[27]	0.0008	114.2	$\pm 1.1$	8.9	No	0
[31]	0.0141	16.25	$\pm 0.5$	–	Yes	2
[33]	0.0370	9.14	$\pm 0.45$	6.85	Yes	2
[35]	0.1010	22.6	$\pm 0.5$	7.4	Yes	2
This work	0.0406	100	$\pm 0.464$	7.966	Yes	2

With reference to Fig. 10, the simulated and measured  $-10$  dB impedance bandwidths are 106.6% (4–13.13 GHz) and 101.9% (3.99–12.28 GHz). The measured and simulated resonant frequencies are in good agreement, but the measured bandwidth is a little smaller than simulated one. The resonant depth of measured reflection coefficient at the low frequency agrees well with the simulated one, while the measured resonant depth deviation is slightly large in the range of 8–11 GHz, which is mainly attributed to the fabrication tolerance. However, the measured impedance bandwidth of proposed antenna has achieved  $|S_{11}| < -10$  dB in the 4–12 GHz, realizing the design goal of proposed antenna bandwidth. Figure 11 plots the measured and simulated gain responses, which are stable at  $8 \pm 0.5$  dBi (4–12 GHz) and  $7.966 \pm 0.464$  dBi (4–12 GHz). The maximum measured gain is 8.43 dBi, which is slightly lower than 8.5 dBi from that of simulated. This may be caused by the measurement errors. As expected, the measured proposed antenna has a little deviation from the simulated one in lower out-of-band frequency, and has about 15.5 dBi out-of-band suppression level in high frequency radiation null. Figure 12 exhibits the normalized measured and simulated H-plane and E-plane radiation patterns of the proposed antenna at 4 GHz, 8 GHz, and 12 GHz, respectively. From both the measured and simulated results, the main beam has good direction and they have slight deviations from the simulated ones.

A comparison between the proposed work and the other reported broadband and filtering antennas is summarized in Table 1. As can be seen from Table 1, the presented antenna here achieves a higher average gain of 7.966 dBi, a flatter gain fluctuation of  $\pm 0.464$  dBi, and the filtering characteristic with out-of-band suppression level of more than 15 dBi than broadband antennas [15, 19, 21, 26, 27]. Compared with the filtering antennas [31, 33], and [35], the proposed antenna has a wider bandwidth of 100% for  $|S_{11}| < -10$  dB. The advantage of the proposed antenna over the above-mentioned

structures is that it can realize broadband, flat gain, and filtering characteristics, simultaneously.

## 4 Conclusion

This article presents a broadband antenna with simultaneous flat gain and filtering characteristic. The basic structure of the antenna consists of a broadband balun, a main elliptic radiator, and a filtering structure. The rectangle slots are loaded on the main radiator to adjust the surface currents phase and attenuate the reverse currents cancellation, so as to improve the gain. Moreover, the cascading of filtering structure can equalize the surface currents amplitude to enable the antenna realize better flat gain response and filtering characteristic. The proposed antenna finally achieves a low gain fluctuation of  $\pm 0.464$  dBi in the 4–12 GHz covering CX-band and a high suppression level of 15.5 dBi in the upper stopband. In particular, the proposed antenna has good potential to be applied as a receiving antenna in high-precision radar sensing system, such as GMTI radar sensing system.

**Acknowledgements** This work is supported by the National Key Research and Development Program of China (Grant No. 2017YFA0204600)

## References

- Chang, E.; Long, S.A.; Richards, W.F.: An experimental investigation of electrically thick rectangular microstrip antennas. *IEEE Trans. Antennas Propag.* **34**(6), 767–772 (1986)
- Schaubert, D.H.; Pozar, D.M.; Adrian, A.: Effect of microstrip antenna substrate thickness and permittivity: comparison of theories with experiment. *IEEE Trans. Antennas Propag.* **37**(6), 677–682 (1989)
- Kacar, M.; Perkowski, C.; Deffenbaugh, P. Booth, J.; Mumcu, G.; Weller, T.: Wideband Ku-band antennas using multi-layer direct digital manufacturing. In: 2017 IEEE International Symposium on



- Antennas and Propagation & USNC/URSI National Radio Science Meeting, 2017. pp. 1243–1244 (2017)
4. He, K.; Gong, S.-X.; Gao, F.: A wideband dual-band magneto-electric dipole antenna with improved feeding structure. *IEEE Antennas Wirel. Propag. Lett.* **13**, 1729–1732 (2014)
  5. Bozdog, G.; Kustepeli, A.: Subsectional tapered fed printed LPDA antenna with a feeding point patch. *IEEE Antennas Wirel. Propag. Lett.* **15**, 437–440 (2016)
  6. Ding, C.; Luk, K.M.: Compact differential-fed dipole antenna with wide bandwidth, stable gain and low cross-polarisation. *Electron. Lett.* **53**(15), 1019–1021 (2017)
  7. Ta, S.X.; Choo, H.; Park, I.: Broadband printed-dipole antenna and its arrays for 5G applications. *IEEE Antennas Wirel. Propag. Lett.* **16**, 2183–2186 (2017)
  8. Abril-García, J.H.; Tapia-Rodríguez, R.E.; García-Juárez, A.; Noriega, J.R.; García-Delgado, L.A.; Leal-Cruz, A.L.; Correa-Mena, A.G.; Zaldívar-Huerta, I.E.; Gómez-Colín, R.: Design of a tapered CPW-fed wideband antenna and its application to multi-channel transmission using a hybrid wireless communication system. *AEU Int. J. Electron. Commun.* **112**, 152966–152976 (2019)
  9. Li, M.; Luk, K.-M.: A differential-fed UWB antenna element with unidirectional radiation. *IEEE Trans. Antennas Propag.* **64**(8), 3651–3656 (2016)
  10. Zeng, J.; Luk, K.-M.: A simple wideband magnetolectric dipole antenna with a defected ground structure. *IEEE Antennas Wirel. Propag. Lett.* **17**(8), 1497–1500 (2018)
  11. Kikuta, K.; Hirose, A.: Compact folded-fin tapered slot antenna for UWB applications. *IEEE Antennas Wirel. Propag. Lett.* **14**, 1192–1195 (2015)
  12. An, W.; Wang, X.; Fu, H.; Ma, J.; Huang, X.; Feng, B.: Low-profile wideband slot-loaded patch antenna with multiresonant modes. *IEEE Antennas Wirel. Propag. Lett.* **17**(7), 1309–1313 (2018)
  13. Liu, S.; Wu, W.; Fang, D.-G.: Single-feed dual-layer dual-band E-shaped and U-slot patch antenna for wireless communication application. *IEEE Antennas Wirel. Propag. Lett.* **15**, 468–471 (2016)
  14. Liu, N.-W.; Zhu, L.; Choi, W.-W.; Zhang, J.-D.: A low-profile differentially fed microstrip patch antenna with broad impedance bandwidth under triple-mode resonance. *IEEE Antennas Wirel. Propag. Lett.* **17**(8), 1478–1482 (2018)
  15. Biswas, B.; Ghatak, R.; Poddar, D.R.: A fern fractal leaf inspired wideband antipodal Vivaldi antenna for microwave imaging system. *IEEE Trans. Antennas Propag.* **65**(11), 6126–6129 (2017)
  16. Gautam, A.K.; Bisht, A.; Kanaujia, B.K.: A wideband antenna with defected ground plane for WLAN/WiMAX applications. *AEU Int. J. Electron. Commun.* **70**(3), 354–358 (2016)
  17. Roy, B.; Bhattacharya, A.; Chowdhury, S.K.; Bhattacharjee, A.K.: Wideband Snowflake slot antenna using Koch iteration technique for wireless and C-band applications. *AEU - Int. J. Electron. Commun.* **70**(10), 1467–1472 (2016)
  18. Okas, P.; Sharma, A.; Das, G.; Gangwar, R.K.: Elliptical slot loaded partially segmented circular monopole antenna for super wideband application. *AEU Int. J. Electron. Commun.* **88**, 63–69 (2018)
  19. Wang, Z.; Yin, Y.; Wu, J.; Lian, R.: A miniaturized CPW-fed antipodal Vivaldi antenna with enhanced radiation performance for wideband applications. *IEEE Antennas Wirel. Propag. Lett.* **15**, 16–19 (2016)
  20. Zang, Y.; Zhai, H.; Xi, L.; Li, L.: A compact microstrip antenna with enhanced bandwidth and ultra-wideband harmonic suppression. *IEEE Trans. Antennas Propag.* **67**(3), 1969–1974 (2019)
  21. Chang, L.; Chen, L.L.; Zhang, J.Q.; Li, D.: A broadband dipole antenna with parasitic patch loading. *IEEE Antennas Wirel. Propag. Lett.* **17**(9), 1717–1721 (2018)
  22. Arrawatia, M.; Baghini, M.S.; Kumar, G.: Differential microstrip antenna for RF energy harvesting. *IEEE Trans. Antennas Propag.* **63**(4), 1581–1588 (2015)
  23. Rashmi; Kumar, A.; Saraswat, K.; Kumar, A.: Wideband circularly polarized parasitic patches loaded coplanar waveguide-fed square slot antenna with grounded strips and slots for wireless communication systems. *AEU Int. J. Electron. Commun.* **114**, pp. 153011–153018 (2020)
  24. Wang, L.; Cheng, Q.; Tang, W.; Yin, X.; Quevedo-Teruel, O.: On the enhancement of scanning and gain flatness of leaky-wave gap-waveguide antennas with glide symmetry. In: 2019 13th European Conference on Antennas and Propagation, EuCAP 2019. pp. 1–4 (2019)
  25. Faenzi, M.; Gonzalez-Ovejero, D.; Maci, S.: Flat gain broadband metasurface antennas. *IEEE Trans. Antennas Propag.* **69**(4), 1942–1951 (2021)
  26. Sun, H.; Ding, C.; Guo, Y. J.; Mittra, R.: A wideband dipole antenna based on a non-uniformly segmented structure. In: 2017 11th European Conference on Antennas and Propagation, EUCAP 2017. pp. 3572–3574 (2017)
  27. Liang, C.-F.; Cheng, C.-H.: A miniaturized antipodal Vivaldi antenna with flat gain for RF energy harvesting. In: 2021 IEEE MTT-S International Wireless Symposium, IWS 2021. pp. 1–3 (2021)
  28. Li, X.; Zhou, H.; Gao, Z.; Wang, H.; Lv, G.: Metamaterial slabs covered UWB antipodal Vivaldi antenna. *IEEE Antennas Wirel. Propag. Lett.* **16**, 2943–2946 (2017)
  29. Teni, G.; Zhang, N.; Qiu, J.; Zhang, P.: Research on a novel miniaturized antipodal Vivaldi antenna with improved radiation. *IEEE Antennas Wirel. Propag. Lett.* **12**, 417–420 (2013)
  30. Sang, L.; Wu, S.; Liu, G.; Wang, J.; Huang, W.: High-gain UWB Vivaldi antenna loaded with reconfigurable 3-D phase adjusting unit lens. *IEEE Antennas Wirel. Propag. Lett.* **19**(2), 322–326 (2020)
  31. Wang, S.; Fan, F.; Gomez-Garcia, R.; Yang, L.; Li, Y.; Wong, S.-W.; Zhang, G.: A planar absorptive-branch-loaded quasi-yagi antenna with filtering capability and flat gain. *IEEE Antennas Wirel. Propag. Lett.* **20**(9), 1626–1630 (2021)
  32. Wei, Z.; Zhou, Z.; Tang, Z.; Yin, J.Y.; Ren, J.; Yin, Y.: Broadband filtering magneto-electronic dipole antenna with quasi-elliptic gain response. *IEEE Trans. Antennas Propag.* **68**(4), 3225–3230 (2020)
  33. Liu, Q.; Zhu, L.; Wang, J.; Wu, W.: A wideband patch and SIW cavity hybrid antenna with filtering response. *IEEE Antennas Wirel. Propag. Lett.* **19**(5), 836–840 (2020)
  34. Liu, G.; Pan, Y.M.; Wu, T.L.; Hu, P.F.: A compact planar quasi-yagi antenna with bandpass filtering response. *IEEE Access.* **7**, 67856–67862 (2019)
  35. Yang, W.; Zhang, Y.; Che, W.; Xun, M.; Xue, Q.; Shen, G.; Feng, W.: A simple, compact filtering patch antenna based on mode analysis with wide out-of-band suppression. *IEEE Trans. Antennas Propag.* **67**(10), 6244–6253 (2019)
  36. Gazit, E.: Improved design of the Vivaldi antenna. *Proc. Inst. Elect. Eng. H.* **135**(2), 89–92 (1988)

Springer Nature or its licensor (e.g. a society or other partner) holds exclusive rights to this article under a publishing agreement with the author(s) or other rightsholder(s); author self-archiving of the accepted manuscript version of this article is solely governed by the terms of such publishing agreement and applicable law.

